Effect of surface texture of precast ultra-high-performance concrete tubes on bond strength with normal concrete fill

Mina Fakeh and Amir Fam

- Ultra-high-performance concrete (UHPC) can be used as stay-in-place structural forms for columns to retain normal-strength concrete cores, but for the two materials to work together effectively, they need to bond well at their interface.
- The authors tested how different interface textures (smooth, bubbled, and corrugated) affected peak and residual bond strength using push-off shear tests.
- Both the bubbled and corrugated surfaces bonded significantly better than smooth surfaces, with medium-sized bubble textures performing best. Adding mesh reinforcement also improved bond strength.
- The authors developed equations for predicting bond strength based on the interface texture, reinforcement used, and NSC strength.

Ultra-high-performance concrete (UHPC) has become a widely favored material for strengthening normal-strength concrete (NSC) through column jacketing[1–4] and for beam strengthening,[5–7] bridge overlays,[8] and connections.[9] For example, UHPC is used to retrofit columns; a UHPC jacket is poured around the NSC column, serving either as a repair system for damaged columns or as a strengthening system for increased load demand. UHPC's excellence in the aforementioned applications is due to its superior durability[10,11] and its mechanical properties that enhance load transfer.[9,12] Furthermore, because using UHPC requires less concrete than conventional methods, it is cost efficient.[5,13]

UHPC's cost-effectiveness is also generating interest for the construction of hybrid members. This involves creating a UHPC stay-in-place form, which is then filled with NSC. For instance, the stay-in-place form for columns is a UHPC tube. This method serves multiple purposes—namely, providing formwork for NSC, which accelerates construction, eliminates temporary formwork, boosts column strength, and protects the NSC core. On one hand, UHPC stay-in-place forms cost more than conventional formwork. On the other hand, the forms also provide additional strength that is not added by conventional formwork. This could lead to an increase in cost-effectiveness when considering the entire system.

In eccentrically loaded columns or beams, the bond between the two concrete types plays a crucial role in enabling the full composite action. Bonding mechanisms include mechanical interlocking, friction, and adhesion. In applications where UHPC is prefabricated, such as stay-in-place forms, mechanical interlocking can be created during fabrication. For example, Fakeh and Fam[14] tested UHPC–NSC beams in flexure with either corrugated or flat interfaces. The authors reported that corrugated interfaces achieved a 29% increase in flexural capacity compared with flat interfaces. Jang et al.[15] investigated the UHPC–NSC shear performance using the push-off test method on flat panels. The tested interfaces include natural surfaces, prefabricated grooves, and surfaces roughened using the waterjet technique. Waterjet surface-roughening significantly enhanced shear capacity, achieving a shear strength of 6.00 MPa (0.87 ksi), while the groove method reached 5.13 MPa (0.74 ksi).[15] Using the same test method, Liu et al.[16] investigated the shear performance of UHPC–NSC interfaces of flat panels using prefabricated UHPC bubble-textured substrates. These substrates helped the system achieve a maximum shear strength of up to 2.72 MPa (0.39 ksi) without dowel bars and up to 3.62 MPa (0.53 ksi) with dowel bars.

The very few available studies on UHPC–NSC interfacial bond were all conducted on flat surfaces and therefore do not account for the additional confinement effect encountered in circular interfaces. In UHPC–NSC columns, for example, the hoop reinforcement ratio also plays a critical role. For unconfined, flat interfaces, the bond between both materials is governed predominantly by pure shear. In contrast, when NSC is confined in push-off testing, a different boundary condition is introduced. Under loading, the NSC core undergoes dilation, which is restrained by the surrounding UHPC jacket. This restraint induces radial stresses at the interface, providing confinement that increases the bond strength. The current study is the first to address this knowledge gap. The study carried out push-off tests on cylindrical stubs of NSC cores cast in UHPC tubes. It introduced a novel corrugated interface and a practical, simple way to produce it in precast UHPC tubes, along with a bubbled interface. The bond strengths of these test interfaces were compared with a smooth interface as a control. The study evaluated the effects on bond strength of hoop reinforcement ratio, fiber type in UHPC, and NSC core strength.

Experimental program

This section outlines the test matrix and the method used to fabricate the specimens. It also presents the properties of the materials used and describes the test setup and instrumentation.

Test matrix

For each specimen, a UHPC cylinder was filled with an NSC core such that both materials were flush on the upper surface while the NSC core was 60 mm (2.4 in.) shorter at the bottom, which created a cavity to allow for slip (**Fig. 1**). **Table 1** shows the test matrix, which contains 46 test specimens and 9 control specimens with a smooth interface from literature.[17] The key parameters (Table 1) were the interface type between UHPC and NSC (smooth, a pattern of near-cylindrical recesses, longitudinal corrugations), reinforcement in UHPC (no mesh, 3 mm [0.12 in.] diame-

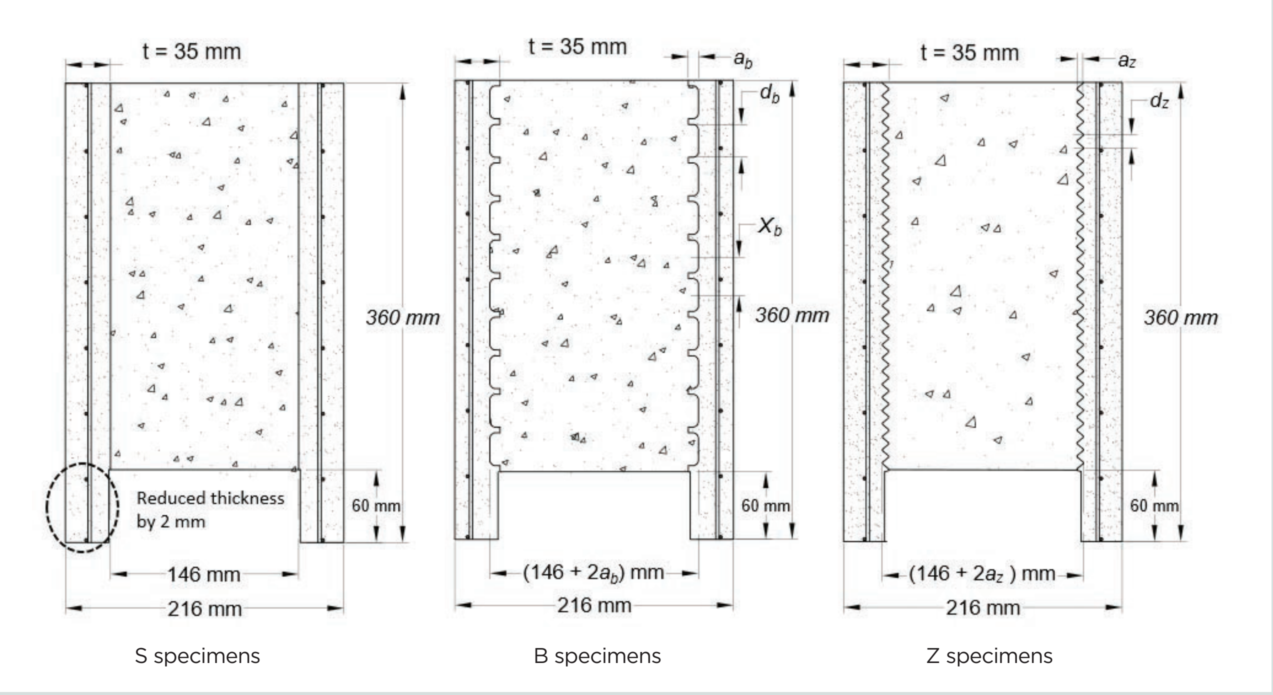

Figure 1. Details of S, B, and Z specimens with 51 × 51 mm (M2) mesh in ultra-high-performance concrete tubes. Note: a_b = bubble rise; a_z = amplitude; d_b = bubble diameter; d_z = corrugation pitch; x_b = center-to-center bubble distance. 1 mm = 0.0394 in.

Table 1. Test matrix and material properties

Specimen	Number	Sample identification	Interface	UHPC hoop reinforcement ratio, %	Fiber type	UHPC $f'_{c,u}$, MPa (SD)	NSC $f'_{c,n}$, MPa (SD)
S (control)	3	S30S*	Natural flat	0	Steel	157.3 (2.6)	31.2 (0.8)
	3	M2-S30S*		0.41		160.4 (2.7)	
	3	M1-S30S*		0.82			
B	1	1B30S	Spherical recesses using bubbles (1B/2B/3B)	0	Steel	151.3 (2.5)	30 (0.51)
	2	2B30S					
	2	3B30S					
	2	M2-1B30S		0.43 to 0.52† (M2 tube)		156.5 (2)	
	2	M2-2B30S					
	2	M2-3B30S					
	2	M2-2B30P			POM	145.3 (1.8)	
	2	M1-1B30S		0.87 to 1.04† (M1 tube)	Steel	159 (1.5)	
	2	M1-2B30S					
	2	M1-3B30S					
	2	M1-2B30P			POM	145.3 (1.8)	
Z	2	1Z30S	Longitudinal corrugations (1Z/2Z/3Z)	0	Steel	153.4 (1.7)	27.8 (0.9)
	2	2Z30S					
	1	3Z30S					
	2	M2-1Z30S		0.42 to 0.43† (M2 tube)	Steel	147 (4.7)	
	2	M2-2Z30S					
	2	M2-3Z30S					
	2	M2-1Z50S					46.5 (2.7)
	2	M2-1Z30P			POM	145.3 (1.8)	30 (0.51)
	2	M1-1Z30S		0.84 to 0.86† (M1 tube)	Steel	155.1 (2.1)	27.8 (0.9)
	2	M1-2Z30S					
	2	M1-3Z30S					
	2	M1-1Z50S					46.5 (2.7)
	2	M1-1Z30P			POM	145.3 (1.8)	30 (0.51)

* Data from Fakeh and Fam (2026)

† Ratio calculated using effective thickness after subtracting volume of bubbles or corrugations.

Note: $f'_{c,n}$ = compressive strength of NSC; $f'_{c,u}$ = compressive strength of UHPC

NSC = normal-strength concrete; POM = polyoxymethylene; SD = standard deviation; UHPC = ultra-high-performance concrete. 1 MPa = 0.145 ksi.

ter steel wire mesh with 51 × 51 mm [2 × 2 in.] openings or 3 mm diameter steel wire mesh with 25 × 25 mm [1 × 1 in.] openings), and the type of fibers used in UHPC (steel or polyoxymethylene [POM]). Although POM fibers reduce the UHPC strength, they are desired for better performance of UHPC in fire.[18] For the corrugated interface specimens, the NSC core design compressive strength also varied (30 or 50 MPa [4.4 or 7.3 ksi]).

Fabrication

The stubs were fabricated by creating the UHPC tubes, which were cured at room temperature using moist burlap for 7 days. This was followed by placing the NSC core. As previously described, the total height of the UHPC tubes H_t was 360 mm (14.17 in.), while the height of the NSC cores was only 300 mm (11.81 in.), which formed an air gap of 60 mm

(2.4 in.) below the core to enable slip. The UHPC wall thickness within the 60 mm height was reduced by 2 mm (0.08 in.) to avoid friction during slip.

The smooth interface of the control specimens (S specimens) was created by using cardboard tubes of two different sizes for fabricating the UHPC tubes. The different sizes created a section with inner and outer dimensions of 146 and 216 mm (5.75 and 8.50 in.), respectively, and a tube thickness t_u of 35 mm (1.38 in.) (Fig. 1). The specimens had different wire mesh hoop reinforcement ratios $\rho_{c,uh}$ (0%, 0.41%, and 0.82%) in the UHPC jacket. The hoop reinforcement ratios are based on the commercially available mesh sizes while ensuring flowability of fresh UHPC. Based on preliminary casting trials, reinforcement ratios exceeding 0.82% resulted in noticeable reductions in workability and difficulties in achieving proper placement, while ratios below 0.41% were considered insufficient to produce enough confinement.

The near-cylindrical recess pattern (bubbled textured) test specimens (B specimens) were created by wrapping bubble-wrap sheets (in three sizes) around the inner cardboard tube of the same size as the control S specimens (**Fig. 2**). While slight variations in bubble size may occur due to the fragility of the Bubble Wrap, these differences were considered negligible and unlikely to affect the consistency of the surface indentations or the overall results.

Table 2 shows the dimensions (parameters) of each textured interface. For B specimens, these are bubble diameter d_b, bubble rise a_b, and center-to-center bubble distance x_b (Fig. 1). Bubble diameter d_b (the main identifier used in the study) was 10 mm (0.39 in.) (Type 1B), 25 mm (1.0 in.) (Type 2B), and 30 mm (1.18 in.) (Type 3B), where the corresponding bubble rise a_b was 4, 8, and 13 mm (0.16, 0.31, and 0.51 in.), respectively. The three specimen types were created with $\rho_{c,uh}$ in the UHPC tube of 0%, 0.43% to 0.52% (M2 jacket), and 0.87% to 1.04% (M1 jacket). The $\rho_{c,uh}$ range is due to the variations in jacket thickness from the bubbles; however, the mesh size was identical for all bubble sizes. The $\rho_{c,uh}$ were calculated using a UHPC equivalent thickness t_e after removing the bubble volume. For the 2B specimens, the fibers varied between steel and POM in the UHPC tubes with M2 and M1 configurations. Figure 2 shows the fabricated specimens, where the inner surface of the UHPC jacket reflects the shape of the Bubble Wrap, after the wraps have been removed.

The longitudinal corrugation patterns (Z specimens) were created using plastic flexible corrugated tubes. Three different pitches were created by stretching the flexible tube to different levels (Fig. 2). The flexible tubes, nearly 0.5 mm (0.02 in.) thick, were slipped around the inner cardboard tube to gain rigidity. Two parameters were used to define corrugations: corrugation pitch d_z, which is the main identifier for the Z specimens, and amplitude a_z (Fig. 1). The d_z values were 6 mm (0.24 in.) (Type 1Z), 10 mm (0.39 in.) (Type 2Z) and

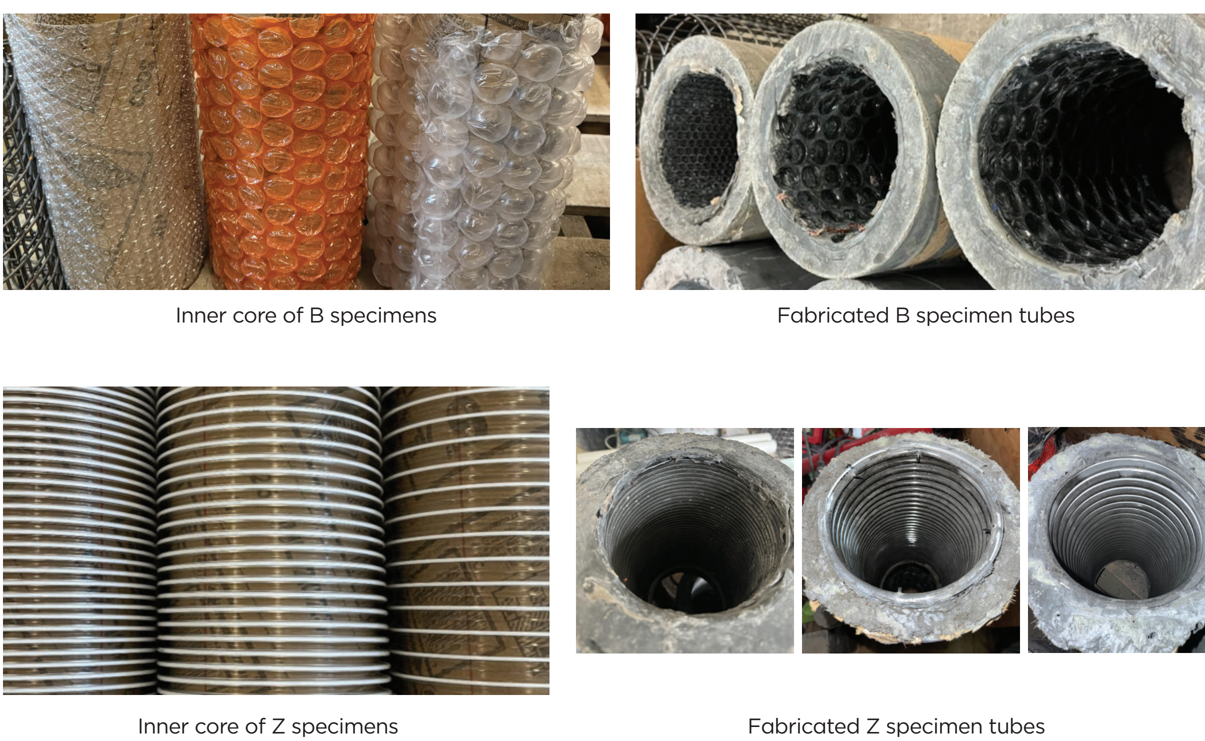

Figure 2. Fabrication of textured interface with inner core of B specimens, fabricated B specimen tubes, inner core of Z specimens, and fabricated Z specimen tubes.

Table 2. Geometric properties of the test interfaces used in this study

B specimens (bubbles)					Z specimens (corrugations)			
Type, number	x_b, mm	d_b, mm	a_b, mm	$\frac{V_b}{A_s}$, mm³/mm²	Type, number	d_z, mm	a_z, mm	$\frac{V_b}{A_s}$, mm³/mm²
1B	12	10	4	2.57	1Z	6	7	2.33
2B	29.5	25	8	5.14	2Z	10	5	2.00
3B	32.5	30	13	8.01	3Z	15	3	1.30

Note: a_b = bubble rise; a_z = amplitude; A_s = interface surface area; d_b = bubble diameter; d_z = corrugation pitch; V_b = volume of bubbles; x_b = center-to-center bubble distance. 1 mm = 0.0394 in; 1 mm² = 0.00155 in.²; 1 mm³ = 0.00006102 in.³

15 mm (0.59 in.) (Type 3Z), which correspond to a_z values of 7, 5, and 3 mm (0.28, 0.20, and 0.12 in.), respectively. The three specimens with profile variations were created with $\rho_{c,uh}$ in UHPC of 0%, 0.42% to 0.43% (M2 jacket), and 0.84% to 0.86% (M1 jacket). Similarly, the reinforcement range arises from reductions in tube thickness due to corrugations. Two separate variations were made from 1Z specimens with M2 and M1 UHPC tubes: the first replaced steel fibers with POM and the second increased NSC compressive strength from 30 to 50 MPa (4.4 to 7.3 ksi). Figure 2 shows the completed UHPC tubes with each corrugation level. The corrugated tubes were left inside.

Material properties

UHPC and NSC To fabricate the UHPC tubes, eight UHPC pours with steel fibers were produced using a commercially available UHPC mixture with 2% fibers by volume. The steel fibers were 0.2 mm (0.008 in.) in diameter and 13 mm (0.51 in.) long. In addition, one pour was produced with 2% POM fibers with dimensions of 0.2 × 12 mm (0.47 in.). The steel fibers have a reported tensile strength of 2850 MPa (413 ksi), whereas the POM fibers have a reported tensile strength of 950 MPa (138 ksi). All UHPC batches were produced using a heavy-duty vertical shaft paddle mixer. The four NSC mixtures were produced using a high-capacity portable mixer. The mixture proportions used for both UHPC and NSC are given in **Table 3**.

Compressive strength was measured for UHPC and NSC in accordance with ASTM C39,[19] using three specimens from each placement. The compressive strength was measured using a compressometer equipped with an attached linear potentiometer to record axial deformation during testing. The device was fixed to the specimen over a defined gauge length, enabling accurate measurement of strain and corresponding stress–strain response (**Fig. 3**). Table 1 shows the average compressive strengths f_c' for UHPC and NSC for all placements in addition to the standard deviations. The average f_c' ranged from 145 to 160 MPa (21.0 to 23.2 ksi) for UHPC and 28 to 31 MPa (4.1 to 4.5 ksi) for NSC of 30 MPa (4.4 ksi) design strength, and 46.5 MPa (6.74 ksi) for NSC of 50 MPa (7.3 ksi) design strength.

Steel mesh Steel wire mesh coupons were tested to evaluate the modulus of elasticity E_s, yield stress f_y, and tensile strength f_u. Figure 3 shows a representative stress–strain curve of the steel mesh. The average values were 199 GPa (28,900 ksi) for E_s, 562 MPa (82 ksi) for f_y, and 632 MPa (92 ksi) for f_u.

Table 3. Ultra-high-performance concrete (UHPC) and normal-strength concrete (NSC) mixture components

Batch	UHPC	NSC (30 MPa strength)	NSC (50 MPa strength)
Mixture components	Cement Water Sand Silica Quicklime Fibers* Liquid NiCal Aluminum Oxide	Cement: 385 kg/m³ Water: 218 kg/m³ w/c: 0.57 Sand: 661 kg/m³ Gravel: 1072 kg/m³ (maximum size: 9.5 mm)	Cement: 418 kg/m³ Water: 217 kg/m³ w/c: 0.52 Sand: 692 kg/m³ Gravel: 1121 kg/m³ (maximum size: 9.5 mm)

*Steel fibers: 0.2 mm in diameter × 13 mm long; POM fibers: 0.2 × 12 mm.

Note: POM = polyoxymethylene; w/c = water-cement ratio. 1 mm = 0.0394 in.; 1 kg/m³ = 1.6875 lb/yd³.

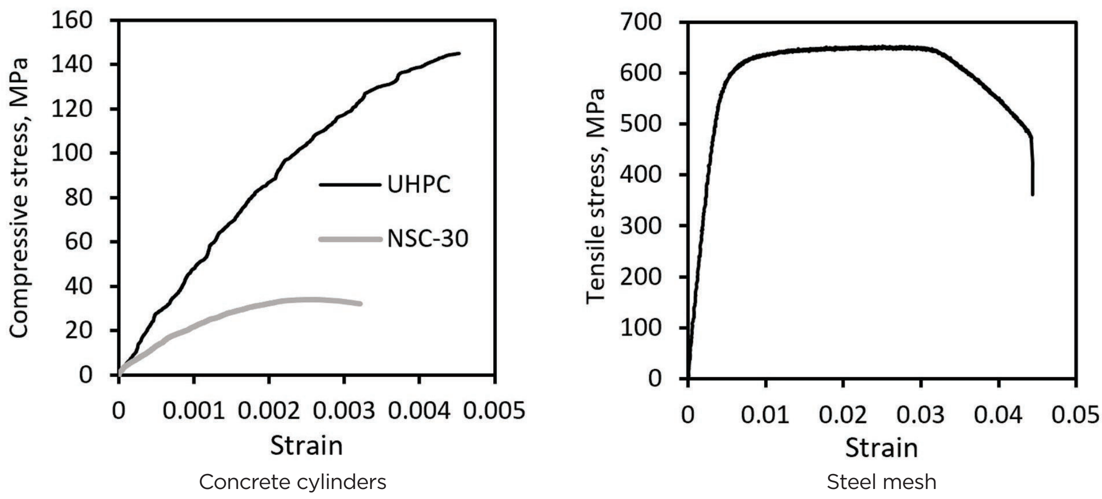

Figure 3. Stress–strain responses for concrete cylinders and steel mesh. Note: NSC = normal-strength concrete; UHPC = ultra-high-performance concrete. 1 MPa = 0.145 ksi.

Test setup

In push-out tests, the UHPC tube was supported at the bottom on the machine base and concentric axial loading was applied at the top on the NSC core using a circular steel plate slightly smaller than the NSC core diameter (**Fig. 4**). A spherical head attached to the testing machine applied loading at a rate of 0.6 mm (0.02 in.) per minute. To monitor slip, three linear potentiometers were installed: one was mounted on the loading plate and measured against a metal bracket glued to the top of the UHPC tube to measure slip on one side of the specimen; two linear potentiometers were mounted to the base of the machine on the other side and measured against a metal bracket glued to the top of the UHPC tube and against the loading plate, respectively, such that the difference was the slip on the other side. The average of the two slip measurements at the diametrically opposite points represented slip at the center. The bond stress τ was calculated from applied load P as presented in Eq. (1):

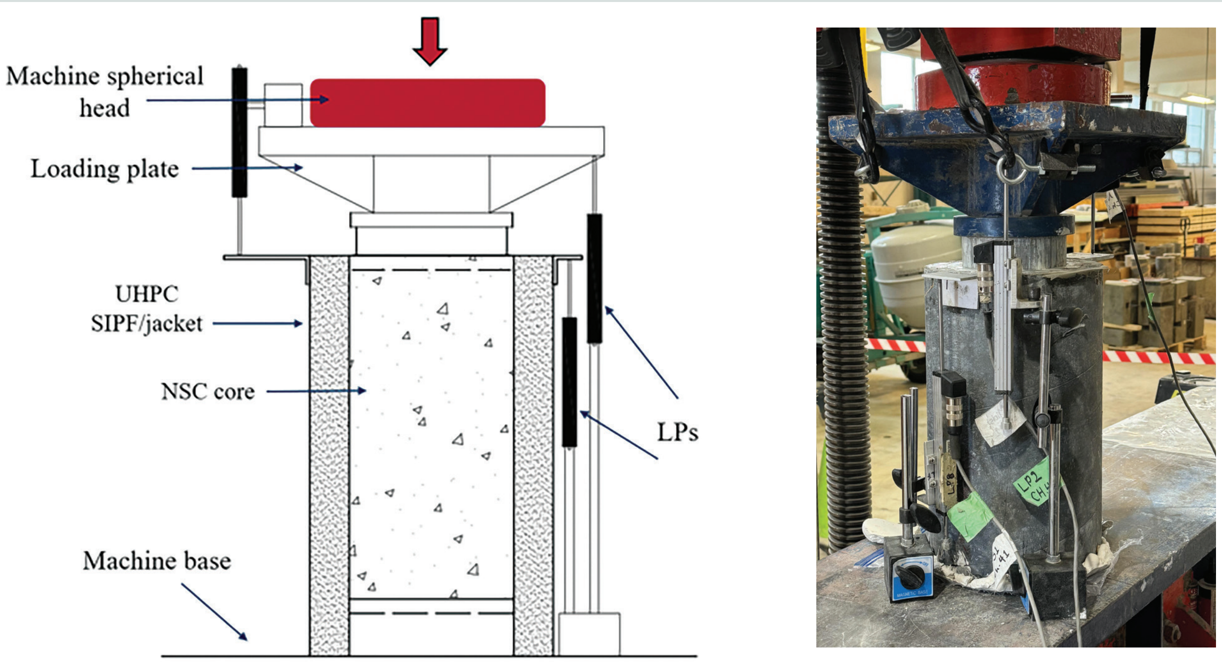

Figure 4. Push-out test setup. Note: LP = linear potentiometer; NSC = normal-strength concrete; SIPF = stay-in-place form; UHPC = ultra-high-performance concrete.

$$\tau = \frac{P}{\pi D_i \left(H_b - S \right)} \quad (1)$$

where

D_i = inside diameter of ultra-high-performance concrete tube

S = slip

H_b = bonded region height

Experimental results

The following sections present results of the experimental program and failure modes, including bond-slip responses. **Table 4** summarizes key results for the two interface types, namely peak bond strength τ_u, residual bond strength τ_r, slip

Table 4. Summary of test results

Specimen	Sample code	τ_u, MPa	τ_u, % increase compared with reference specimens	τ_r, MPa	S_u, mm	Failure mode (behavior type*)
S (control)	S30S	2.03	Reference (no mesh)	1.73	1.57	S
	M2-S30S	2.00	Reference (M2)	1.83	2.01	S
	M1-S30S	2.24	Reference (M1)	1.74	0.24	S
B	1B30S	2.97	+47	0.49	0.60	SP-N (A)
	2B30S	3.80	+88	0.13	0.21	SP-N (A)
	3B30S	2.61	+29	0.05	0.50	SP-N (A)
	M2-1B30S	4.40	+120	1.76	0.75	SP-N (A)
	M2-2B30S	4.24	+112	0.22	0.59	SP-N (A)
	M2-3B30S	4.28	+113	0.23	0.78	SP-N (A)
	M2-2B30P†	3.13	n/a	1.16	0.56	SP-N (A)
	M1-1B30S	4.28	+91	1.94	0.45	SP-N (A)
	M1-2B30S	4.90	+119	0.37	0.76	SP-N (A)
	M1-3B30S	4.82	+115	0.31	1.01	SP-N (A)
	M1-2B30P	3.87	n/a	1.32	1.05	SP-N (A)
Z	1Z30S	2.84	+40	0.97	2.7	SP-NU (C)
	2Z30S	2.92	+44	0.2	2.8	SP-N (C)
	3Z30S	2.12	+4.7	0.9	1.2	SP-S (D)
	M2-1Z30S	2.91	+45	0.35	1.8	SP-NU (D)
	M2-2Z30S	3.41	+70	0.9	2.2	SP-N (C)
	M2-3Z30S	2.81	+40	0.23	1.2	SP-S (D)
	M2-1Z50S	3.55	n/a	n/a	2.3	SP-NU (D)
	M2-1Z30P	1.55	n/a	1.00	13.4	S-NU (B)
	M1-1Z30S	3.27	+46	0.65	2.4	SP-NU (D)
	M1-2Z30S†	3.68	+64	0.51	2.4	SP-N (D)
	M1-3Z30S	3.99	+78	0.31	2.2	SP-N (C)
	M1-1Z50S	3.86	n/a	n/a	2.1	SP-NU (D)
	M1-1Z30P†	2.08	n/a	1.32	12.8	S-NU (B)

*Behavior type as defined in Fig. 7.

†One of the two specimens were defective during fabrication.

Note: n/a = not applicable; NSC = normal-strength concrete; S = slippage of NSC core, with microcracks in UHPC jacket; SP-N = slippage of NSC core, splitting of the UHPC jacket, in addition to NSC shearing; SP-NU = slippage of NSC core, splitting of the UHPC jacket, in addition to a mix of NSC and UHPC shearing; SP-S = slippage of NSC core, with splitting of the UHPC jacket; UHPC = ultra-high-performance concrete. 1 mm = 0.0394 in.; 1 MPa = 0.145 ksi.

at peak bond strength S_u, failure modes, type of bond-slip response, and percentage increase in τ_u relative to control specimens.

Results: B specimens

Failure modes **Figure 5** presents the observed representative failure modes for B specimens with M2 reinforcement, which are the same for specimens with no mesh or with M1 reinforcement. All B specimens exhibited a consistent failure pattern, identified as SP-N (**Fig. 6**). The primary feature of this mode was the longitudinal splitting of UHPC tubes due to the shearing of the near-cylindrical protrusions of the NSC core that filled the recesses formed in the UHPC tube by the Bubble Wrap (Fig. 6). Sliding of the round protrusions before shearing produced vertical slip and exerted

10 mm bubbles (steel fibers) | 25 mm bubbles (steel fibers) | 30 mm bubbles (steel fibers) | 25 mm bubbles (POM fibers)

Figure 5. Failure mode of B specimens with M2 jacket. Note: POM = polyoxymethylene. 1 mm = 0.0394 in.

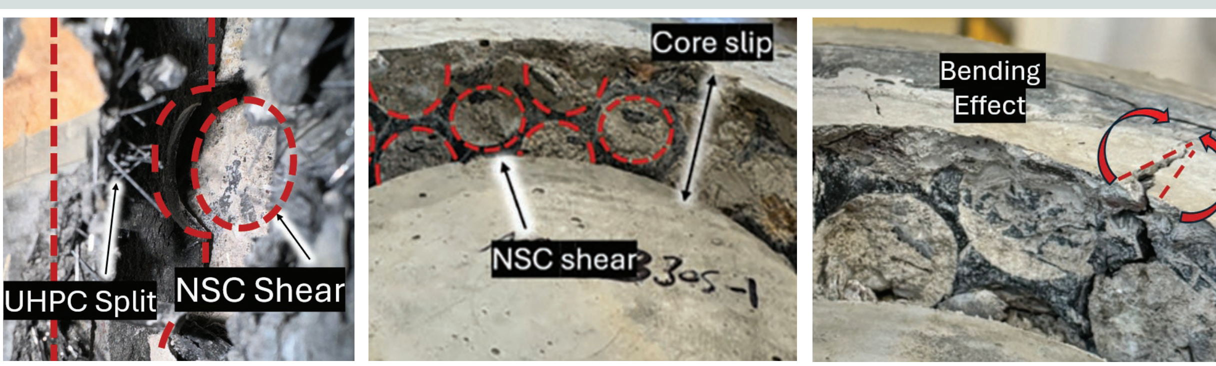

Splitting plane | Interface | Opposite side of the splitting plane

Figure 6. B specimens failure mode SP-N with splitting of the ultra-high-performance concrete tube and shearing of the normal-strength concrete bubbles shown at the splitting plane, interface, and opposite side of the splitting plane. Note: NSC = normal-strength concrete; UHPC = ultra-high-performance concrete.

radial pressure that caused hoop tensile stress and splitting of the UHPC tube at one location. In the prepeak region, this slip was resisted by the circumferential tensile capacity of the UHPC.

In a previous study, the authors reported a circumferential tensile strength of up to 8.25 MPa (1.2 ksi) for steel fiber–reinforced UHPC rings extracted from tubes similar to those investigated in this study.[20] Splitting initiated once the induced hoop tensile stresses exceeded this first-cracking tensile capacity, after which the crack propagated as the UHPC transitioned into the localization phase of its tensile response, resulting in longitudinal splitting of the UHPC tube. During postpeak loading, the UHPC tube on the opposite side of the splitting crack experienced a localized bending crack because of the tube opening (Fig. 6).

The extent of splitting failure was found to be strongly correlated to the size of the bubbles and the mesh size in the jacket. For instance, specimens with smaller bubbles (1B) exhibited only partial splitting and the UHPC tube remained largely intact. This can be attributed to the smaller reduction in UHPC tube thickness, together with the smaller bearing against the tube, compared with specimens with larger bubbles (2B and 3B), which experienced full split at peak load, including the rupture of steel mesh. For 2B specimens with POM fibers, the tube cracked fully, but the mesh remained intact (Fig. 5).

Bond-slip response **Figure 7** shows an idealized bond-slip response of all B specimens, referred to as Type A (see the "Failure mode (behavior type)" column in Table 4). **Figure 8** shows the experimental bond-slip responses for the three

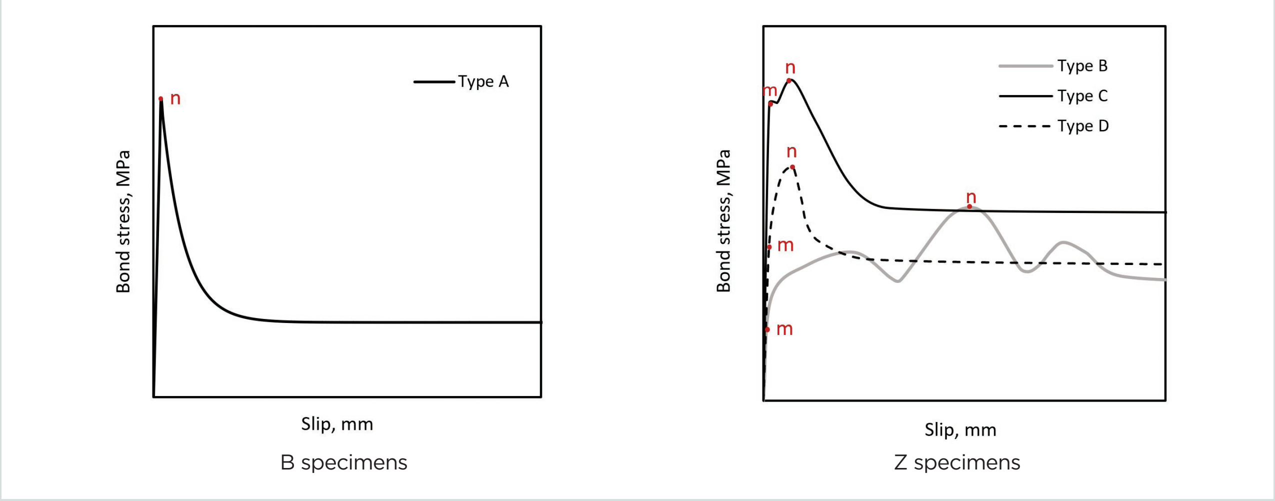

Figure 7. Typical bond-slip responses of B specimens and Z specimens. Note: 1 mm = 0.0394 in.; 1 MPa = 0.145 ksi.

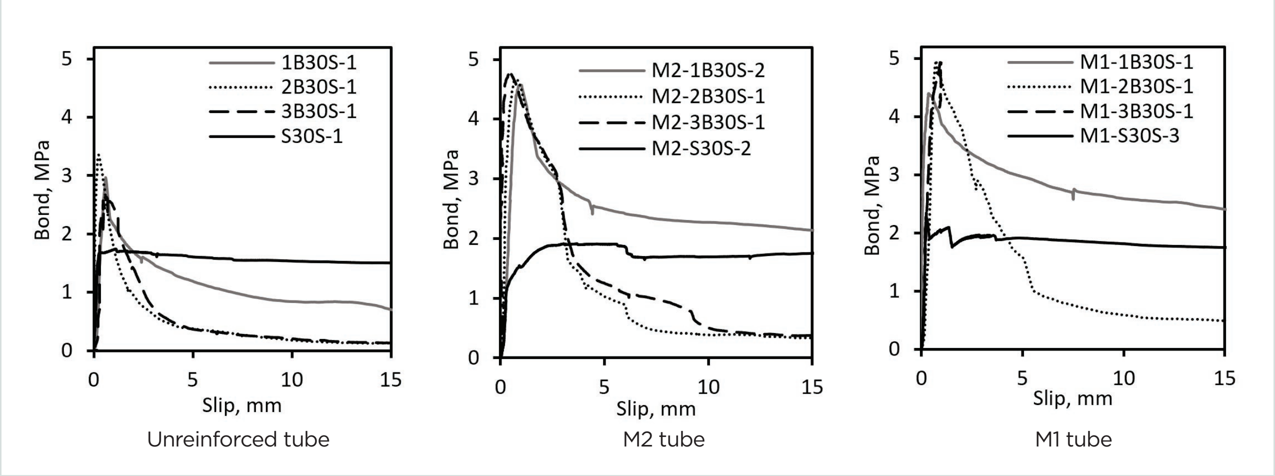

Figure 8. Bond-slip responses of B specimens with unreinforced tube, M2 tube, and M1 tube. Note: 1 mm = 0.0394 in.; 1 MPa = 0.145 ksi.

bubble sizes and different mesh reinforcement ratios, and **Fig. 9** shows the effect of changing fiber type for specimen Type 2B on the response. The bond-slip behavior of the B specimens with steel-fiber UHPC tubes exhibited the following behaviors:

From the origin to point n (as labeled in Fig. 7), the specimens exhibited an initial linear relationship with a few vertical hairline cracks developing around the UHPC tube. This phase, between the start of the test until its peak, was governed primarily by mechanical interlocking through the textured interface and, to a minor extent, by adhesion.

At peak, the bubble protrusions experienced shearing, which prompted slippage and splitting of the tube due to fiber pullout and mesh rupture. In the 1B specimens, the tube experienced partial splitting, where steel fibers and mesh continued to bridge the crack.

Beyond point n, the response transitioned into a softening phase, where bond stress rapidly decreased with slip. This postpeak behavior reflected the loss of interfacial shear resistance due to mechanical interlocking and progressive splitting of the UHPC. The bond became governed primarily by friction enabled by some confinement from the remaining hoop stiffness of the tube (if not fully split [Fig. 5]) or by its bending stiffness (if fully split [Fig. 5 and 6]). Ultimately, bond stress stabilized at a residual value.

Peak bond strength **Figure 10** shows the effects of $\rho_{c,uh}$ and d_b in the UHPC tube on τ_u. For test specimen 1B (unreinforced), τ_u increased by 47% compared with the unreinforced S specimen (control). Including the M2 and M1 meshes ($\rho_{c,uh}$ = 0.43% and 0.87% reinforcement, respectively) increased τ_u by 120% and 91%, respectively, relative to their S specimen counterparts.

The 2B specimens showed the highest improvements of τ_u with 88%, 112%, and 119% increases over their S specimen counterparts with no mesh, M2 mesh, and M1 mesh, respectively. The 2B specimens were fabricated using POM fibers. For the same tube $\rho_{c,uh}$ of 0.46% and 0.93%, τ_u decreased by 26% and 21%, respectively, compared with the corresponding 2B specimen with steel fibers. This comparison highlights the superiority of steel fibers in enhancing bond performance by increasing UHPC tensile strength. For the 3B specimens, τ_u increased by only 29%, 113%, and 115% (no mesh, M2 mesh, and M1 mesh, respectively) compared with their S specimen counterparts.

These results show that both bubble size and $\rho_{c,uh}$ in the UHPC tube affect τ_u. **Figure 11** plots this triaxial relationship. Liu et al.[16] recommended Eq. (2) for shear/bond strength τ_{uo} of a flat (unconfined) bubble-textured interface, which neglects the effect of confinement and adhesion. Their recommendation was based on UHPC–NSC push-off tests conducted on bubble-textured UHPC substrates with NSC placed after UHPC and vice versa, all without confinement.[16] To incorporate the effects of confinement due to curvature and hoop reinforcement, Eq. (3) introduces confinement factor K_b, which is obtained from fitting the triaxial data in Fig. 11 (Eq. [4]); in all cases, K_b surpassed 1.0. Shear/bond strength is sometimes related directly to the compressive strength of the weaker NSC $f'_{c,n}$; however, the strength value in this study is dependent on many variables: d_b, a_b, first cracking strength of UHPC (a function of $\sqrt{f'_{c,u}}$), outer diameter-to-equivalent thickness ratio D_o/t_e, and the tube's $\rho_{c,uh}$. It is worth noting that previous studies have used the term $\sqrt{f'_{c,u}}$ to estimate the first cracking strength[21] and tensile strength[20] of UHPC. To capture all of the aforementioned parameters, Eq. (2) includes d_b and $f'_{c,n}$. Equation (4) includes the remaining parameters. Figure 11 shows that nearly all experimental values lie within the ±15% bounds, indicating very good predictive capability.

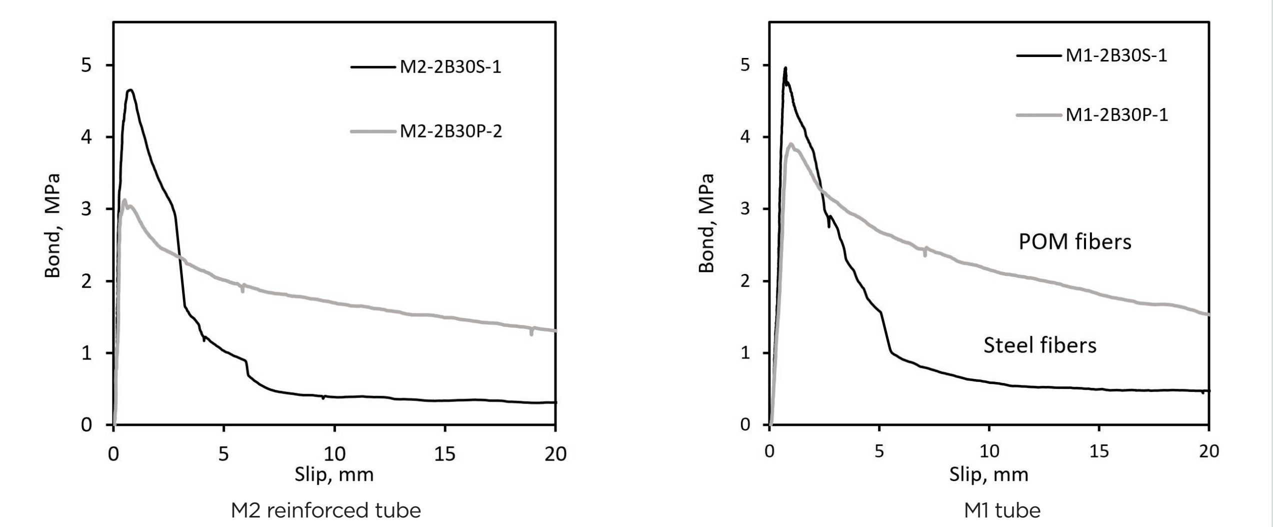

Figure 9. Effect of fiber type on bond-slip of 2B specimens with M2 reinforced tube and M1 tube. Note: POM = polyoxymethylene. 1 mm = 0.0394 in.; 1 MPa = 0.145 ksi.

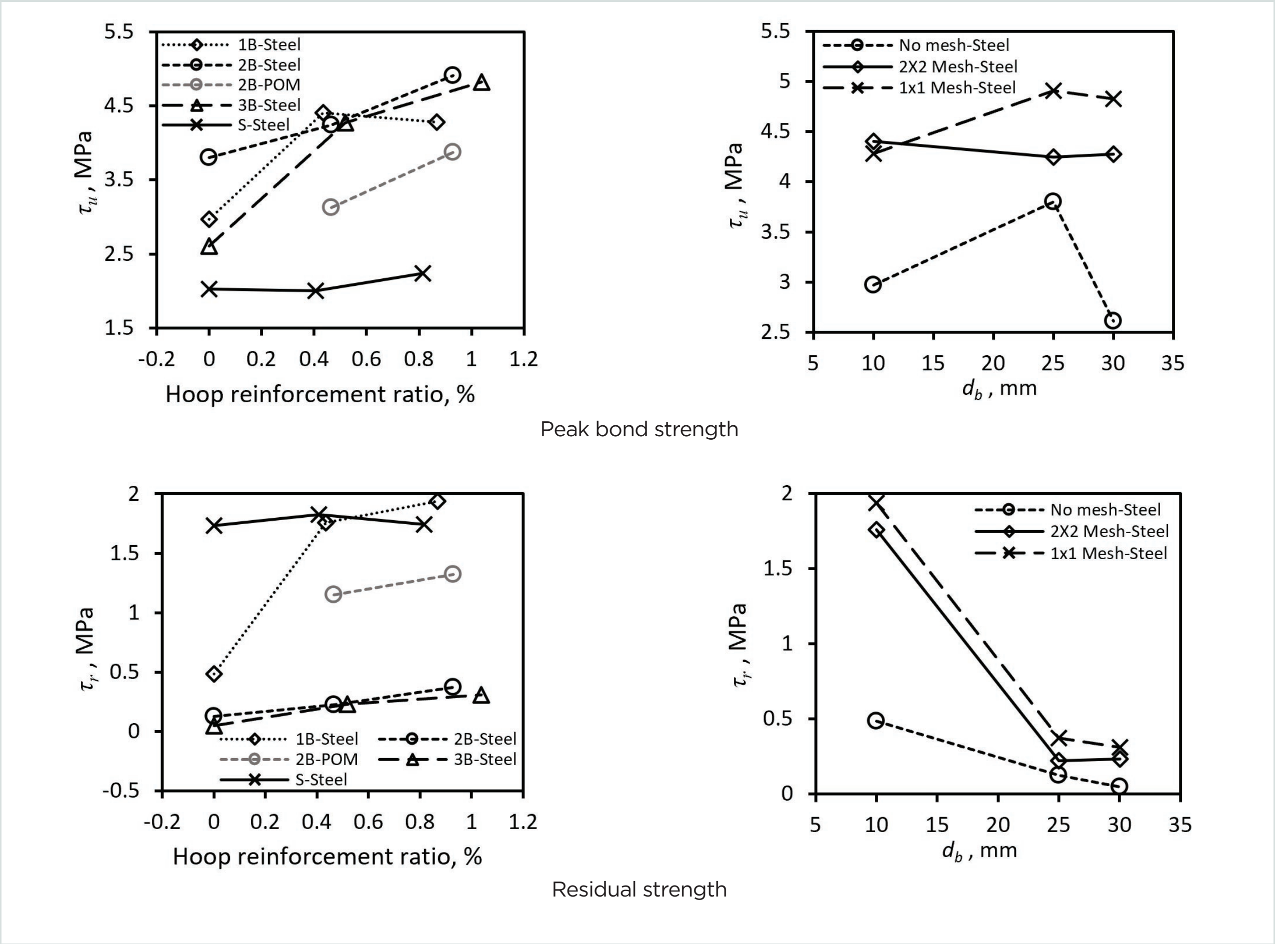

Figure 10. Effect of hoop reinforcement ratio and bubble diameter d_b on peak bond strength τ_u and on residual strength τ_r in B specimens. Note: POM = polyoxymethylene. 1 mm = 0.0394 in.; 1 MPa = 0.145 ksi.

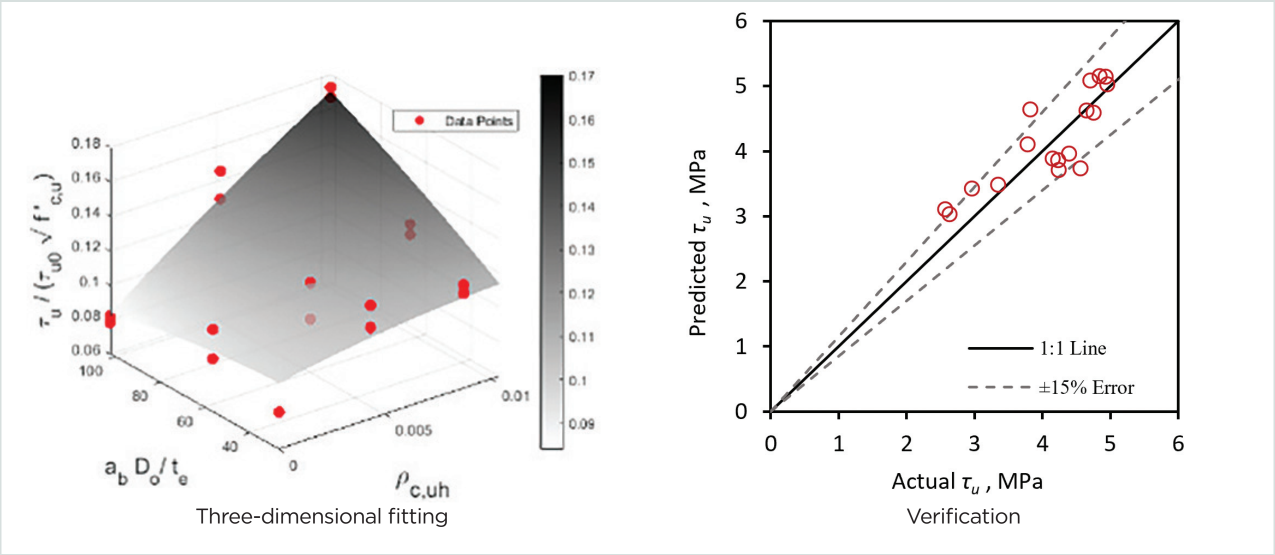

Figure 11. Effect of bubble size and hoop reinforcement on peak bond strength three-dimensional fitting and verification. Notes: a_b = bubble rise; D_o/t_e = outer diameter-to-equivalent thickness ratio; $f'_{c,u}$ = compressive strength of UHPC; $\rho_{c,uh}$ = hoop reinforcement ratio; τ_u = peak bond strength; τ_{uo} = reference shear/bond strength. 1 MPa = 0.145 ksi.

$$\tau_{uo} = 0.15 f'_{c,n} \frac{A_{b,t}}{A_s} \quad (2)$$

where

$f'_{c,n}$ = compressive strength of NSC

$A_{b,t}$ = bubble area at shear level

A_s = interface surface area

$$\tau_u = K_b \tau_{uo} \quad (3)$$

$$K_b = \sqrt{f'_{c,u}} \left(0.09 \rho_{c,uh} a_b \frac{D_o}{t_e} - 93 \rho_{c,uh}{}^2 + 0.094 \right); R^2 = 0.85 \quad (4)$$

where

$f'_{c,u}$ = compressive strength of UHPC

Residual bond strength Figure 10 illustrates the influence of $\rho_{c,uh}$ on τ_r. In general, τ_r increased with $\rho_{c,uh}$. This enhancement can be attributed to the improved residual hoop tensile capacity and frictional resistance mobilized after τ_u, owing to the presence of the wire mesh. As Fig. 10 also shows, increasing d_b resulted in a reduction of τ_r. This trend is primarily associated with the reduced hoop tensile capacity after peak bond, which decreases as the UHPC at the splitting area becomes thinner. However, τ_r is almost always lower in the control (with a smooth interface).

For 1B specimens, the UHPC jacket exhibited splitting, with no evidence of mesh rupture, which resulted in higher τ_r of 0.49 to 1.94 MPa (0.07 to 0.28 ksi), directly proportional to $\rho_{c,uh}$. For larger bubbles (2B and 3B), τ_r approached zero, showing only a slight increase with $\rho_{c,uh}$. This is attributed to rupture of the wire mesh at the peak load, leaving less friction between the sheared NSC bubbles. For 2B specimens with POM fibers, the tube exhibited partial splitting, comparable with that observed in the 1B steel-fiber specimens.

Results: Z specimens

Failure modes **Figure 12** illustrates the failure modes of Z specimens, which are also listed in Table 4. The first term of the failure mode code indicates the UHPC tube failure

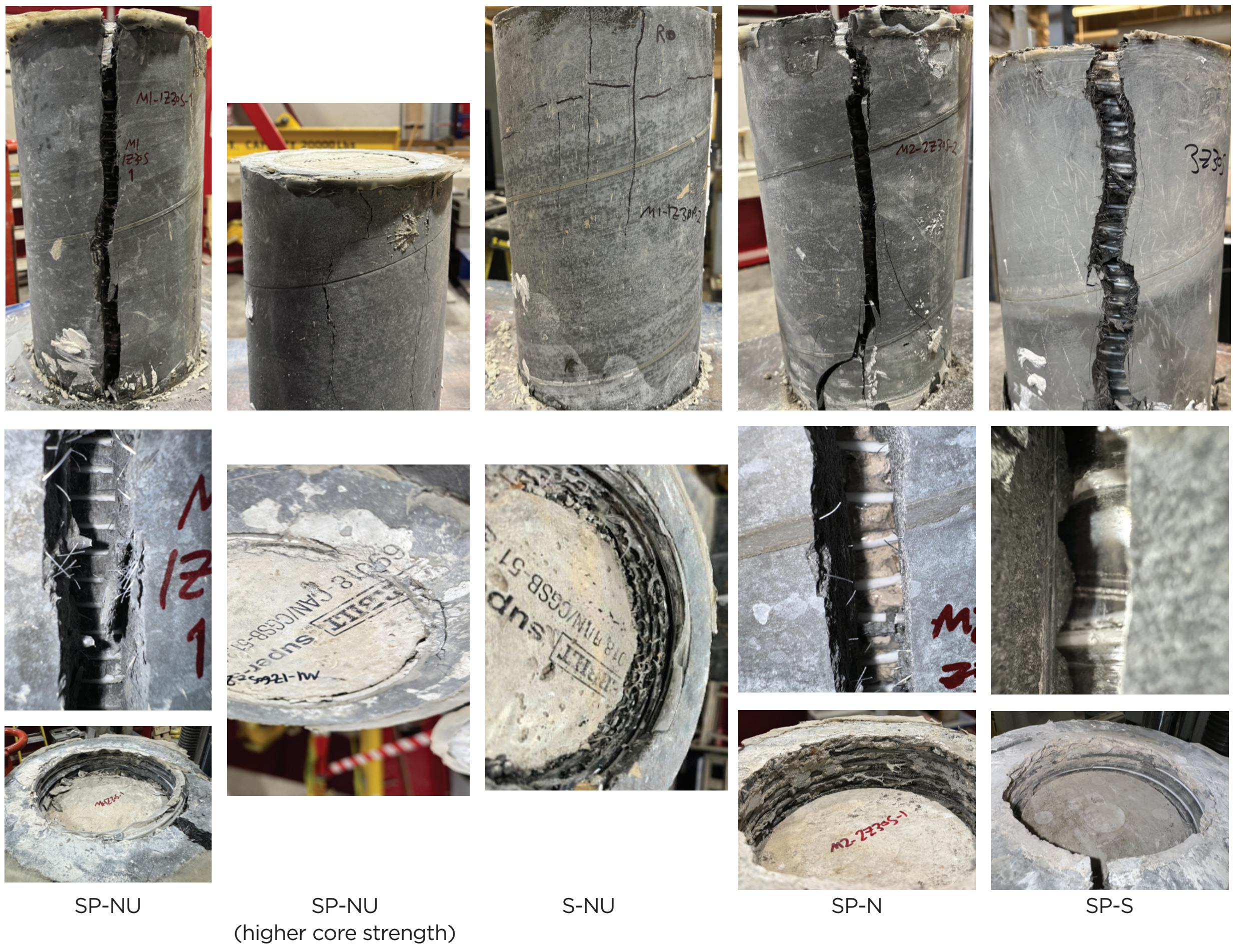

Figure 12. Failure modes of Z specimens.

condition, while the second term indicates interface condition. Unlike B specimens, Z specimens exhibited five different failure modes, which depend mainly on corrugation pitch d_z.

Regardless of UHPC reinforcement level, specimens with 6 mm (0.24 in.) d_z (1Z specimens) with steel fibers exhibited failure mode SP-NU (Fig. 12), characterized by splitting of the UHPC tube (SP), accompanied by mixed shearing of NSC (N) and UHPC (U) circular ribs at the interface due to their small pitch. NSC shearing was visible at the top, while UHPC shearing was visible both at the top and through the splitting crack. Horák et al.[22] evaluated the bond between NSC and UHPC with cone-shaped keys, which demonstrated a similar failure mode with combination shearing of NSC and UHPC cones.

For 1Z specimens with higher NSC strength (46.5 MPa [6.74 ksi]), the specimens experienced the same failure mode; however, the top slip was much less and did not progress further after peak (Fig. 12). In addition, the UHPC splitting was not full. The same specimen type, but with POM fibers in the UHPC, experienced a similar failure mode S-NU (Fig. 12). The core slipped (S) without the jacket splitting but experienced multiple uniformly distributed horizontal and vertical hairline cracks on the outer surface.

Specimens with 10 mm (0.39 in.) d_z (2Z specimens) exhibited a similar failure mode as B specimens in that shear resistance was carried by the NSC ribs. The failure mode SP-N is described by splitting of UHPC tube (SP) accompanied by shearing of the NSC (N) ribs (Fig. 12).

Specimens with 15 mm (0.59 in.) d_z and no hoop or M2 mesh reinforcement (3Z specimens) exhibited a slightly different failure mode SP-S, characterized by splitting of UHPC tube (SP) with slippage of the NSC core, where the NSC ribs slipped (S) over the UHPC ribs without shearing of any of the ribs (Fig. 12). This behavior is attributed to the large d_z with small amplitude a_z, which led to a reduced shear transfer ability because of the shallow interlocking. In specimens 3Z with M1 tubes, failure mode was SP-N, where hoop tensile capacity increased, preventing core slippage and causing a failure with shearing of NSC ribs and tube splitting.

Bond-slip response Figure 7 shows the three types (B, C, and D) of bond-slip behaviors exhibited by the Z specimens. **Figures 13** and **14** present the Z specimens' three types of bond-slip responses. Type B, observed in specimens with POM fibers, is characterized by a linear increase in bond stress up to point m, governed by mechanical interlock. Beyond point m, the bond stress oscillated toward a peak and then declined (Fig. 7). Each drop corresponded to the formation of several hairline vertical cracks in the UHPC tube followed by a subsequent recovery in bond stress.

Response Types C and D exhibited patterns similar to pattern A but differed in their prepeak behaviors. The following behaviors characterized response Type C:

- The specimens exhibited a linear relation from the origin up to point m with no noticeable separation at the top but multiple hairline cracks on the UHPC surface. Bond in this stage was governed by mechanical interlock.
- At point m, visible slip and separation were observed at the top as the NSC core began to detach from the UHPC tube while the ribs were still interlocked. This separation coincided with the appearance of a vertical fine crack.
- Between points m and n, the NSC core continued to slip while bond stress increased at a reduced stiffness to τ_u. Beyond point n, bond stress dropped sharply because of the ribs shearing until stabilizing at τ_r (Fig. 7). At this stage, mechanical interlocking was replaced by friction along the broken ribs.

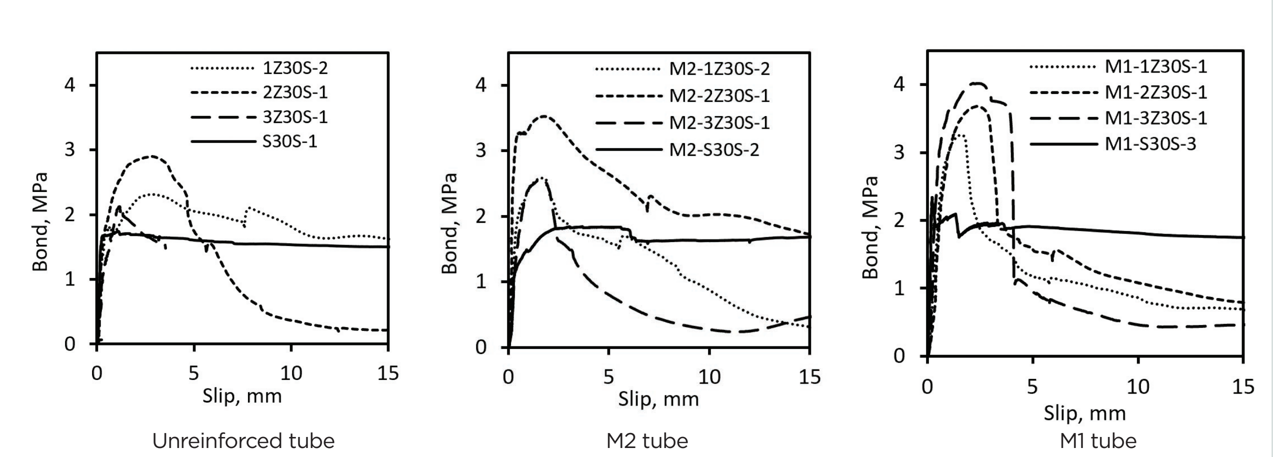

Figure 13. Bond-slip responses of Z specimens with unreinforced tube, M2 tube, and M1 tube. Notes: 1 mm = 0.0394 in.; 1 MPa = 0.145 ksi.

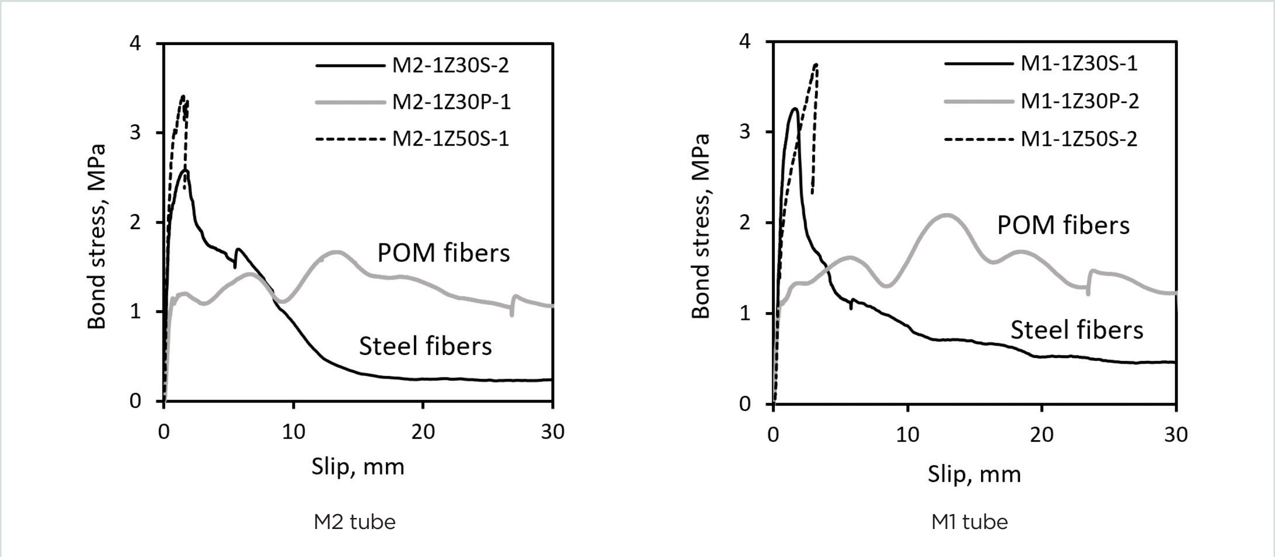

Figure 14. Bond-slip responses of 1Z specimens with M2 and M1 tubes. Note: POM = polyoxymethylene. 1 mm = 0.0394 in.; 1 MPa = 0.145 ksi.

Type D differed from Type C primarily between points m and n, where the transition was more gradual, and no distinct prepeak cracking occurred other than hairline cracks.

Specimens 1Z exhibited Type C behavior when the tube contained no wire mesh and Type D when the mesh was introduced, regardless of $\rho_{c,uh}$, because of the increased hoop strength, which prevented prepeak splitting. Specimens 2Z without mesh and with M2 reinforcement displayed Type C behavior; the tube cracked slightly near the peak load. When M1 with higher $\rho_{c,uh}$ was used, Type D behavior was observed and the enhanced hoop stiffness prevented premature cracking, similar to 1Z specimens. Specimens 3Z exhibited Type D behavior for specimens with no mesh and with M2 reinforcement because they failed at the first cracking with no further shear capacity from the ribs. For the case of the M1 tube, behavior was Type C; the tube cracked slightly but continued to carry load.

Peak bond strength The corrugation pitch d_z directly influenced the extent of mechanical interlock and shear transfer, establishing a clear proportional relationship between d_z and peak bond strength τ_u. **Figure 15** shows the effects of $\rho_{c,uh}$ and d_z on τ_u. Generally, τ_u increased with $\rho_{c,uh}$ but at varying degrees and rates. It is worth noting that specimens with M1 reinforcement exhibited a nearly linear increase in τ_u with increasing d_z because of the same failure mode observed across all M1 specimens with steel fibers.

Compared with the smooth interface (S specimens), the incorporation of corrugations at the UHPC–NSC interface led to notable increases in τ_u. For the 1Z specimens without mesh reinforcement, with M2 mesh, and with M1 mesh, average τ_u were 2.84, 2.91, and 3.27 MPa (0.41, 0.42, and 0.47 ksi), representing increases of 40%, 45%, and 46%, respectively.

The 2Z specimens exhibited the greatest combined enhancements in τ_u, with average values of 2.92, 3.41, and 3.68 MPa (0.42, 0.49, and 0.53 ksi), corresponding to increases of 44%, 70%, and 64% relative to their smooth-interface counterparts with no mesh, M2 mesh, and M1 mesh, respectively.

On the other hand, 3Z specimens, characterized by the largest d_z and smallest a_z, reached average τ_u values of 2.12, 2.81, and 3.99 MPa (0.31, 0.41, and 0.58 ksi) with no mesh, M2 mesh, and M1 mesh, respectively. This represents significant increases of 4.7%, 40%, and 78% in τ_u compared with the respective S specimens. The smaller improvements in the specimens with no mesh and M2 jackets can be attributed to their distinct failure modes where NSC cores experienced slippage, triggering splitting of the UHPC tube before the corrugation could mobilize its shear resistance (Fig. 12). Consequently, the tube's hoop strength was the governing contributor, as opposed to both the hoop strength and shear capacity of the ribs. In contrast, the 3Z specimens with M1 jacket exhibited a different behavior; under stronger confinement, the large corrugations developed shear resistance as the NSC ribs sheared rather than slipped against the UHPC ribs. This more-favorable failure mechanism enabled full mechanical interlock, resulting in the highest increase in τ_u (78%) among all Z specimens.

The 1Z specimens incorporating POM fibers or a higher-strength NSC core (46.5 MPa [6.74 ksi]) exhibited trends parallel to those of the 1Z specimens with steel fibers and 30 MPa (4.4 ksi) NSC, as shown in Fig. 15 but with different bond strengths. The POM fiber specimens showed average τ_u values of 1.55 and 2.08 MPa (0.22 and 0.30 ksi) with M2 and M1 reinforcements, respectively—a decrease in τ_u of 47% and 36%, respectively, relative to the steel-fiber counterparts. On the other hand, the average τ_u values of specimens with

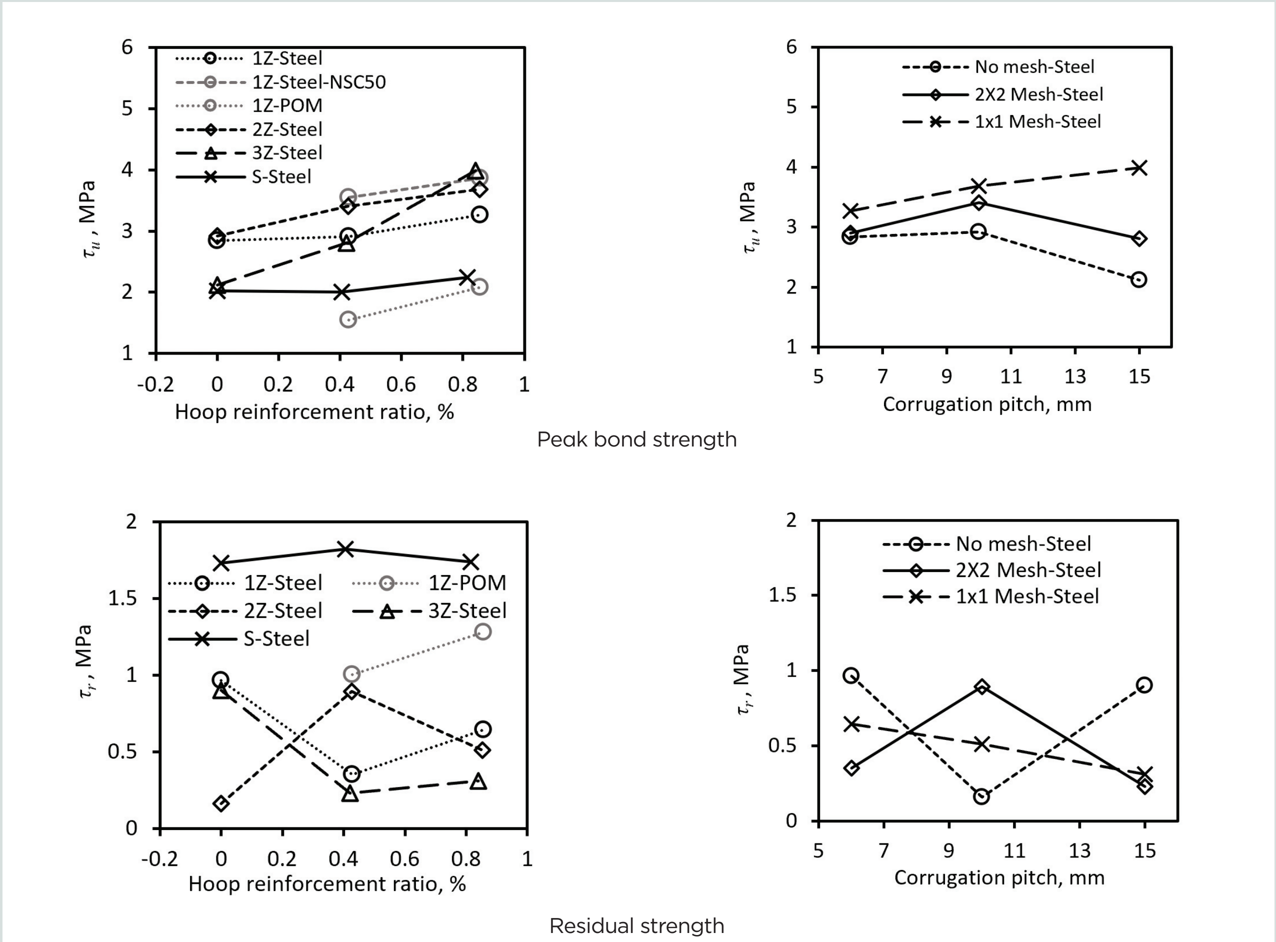

Figure 15. Effect of hoop reinforcement ratio and corrugation pitch on peak bond strength τ_u and on residual strength τ_r in Z specimens. Note: POM = polyoxymethylene. 1 mm = 0.0394 in.; 1 MPa = 0.145 ksi.

the higher-strength NSC core and steel fibers were 3.55 and 3.86 MPa (0.51 and 0.56 ksi), corresponding to an increase of 22% and 18%, respectively, compared with a similar specimen type with 30 MPa core strength.

Residual bond strength Figure 15 also shows the effect of $\rho_{c,uh}$ on τ_r. No clear trend is observed because the specimens exhibited different failure modes and bond-slip responses. Similarly, no clear trend emerges of the effect of d_z on τ_r, except for the M1 specimens as they all share a consistent failure mode and comparable bond-slip behavior. For these specimens, τ_r decreases slightly, from 0.65 to 0.31 MPa (0.09 to 0.04 ksi), with d_z increasing from 6 to 15 mm (0.24 to 0.59 in.).

Comparison of bubbled and corrugated interfaces

Peak bond strength **Figure 16** shows a comparison of τ_u values between all B specimens, Z specimens, and S specimens. The figure highlights that $\rho_{c,uh}$ affects τ_u more significantly with deformed interfaces (both bubbles and corrugations) than with a smooth interface because of the induced internal radial pressure associated with mechanical interlock. The figure also shows that bubble-textured interfaces performed better than corrugated ones, with higher τ_u for both steel and POM fibers (up to 120% compared with 78% for the same hoop reinforcement). This increase is likely due to the larger overall volume of bubble deformations per unit area: 2.6 to 8.0 mm^3/mm^2 (0.10 to 0.31 in.^{3}/in.^{2}) for bubbles compared with only 1.3 to 2.3 mm^3/mm^2 (0.05 to 0.09 in.^{3}/in.^{2}) for corrugations (Table 2).

Bond-slip response For the B specimens, the bond-slip curve remains linear up to the peak, followed by a sharp drop corresponding to adhesion loss and UHPC splitting. In contrast, the Z specimens deviate from linearity before the peak and exhibit a plateau at the peak, reflecting the gradual engagement of corrugations. Table 4 presents the slip at peak S_u values, which are consistently higher for specimens exhibiting Type D behavior than for Type A. This suggests that a corrugated interface allows additional slip before full bond failure. Figure 16 shows the range of S_u values among all steel-fiber specimens for both B and Z specimens. The S_u for Z specimens ranges from 1.2 to 2.8 mm (0.05 to 0.11 in.) for steel-fiber specimens and up to 13.4 mm (0.53 in.) for POM, and for B specimens

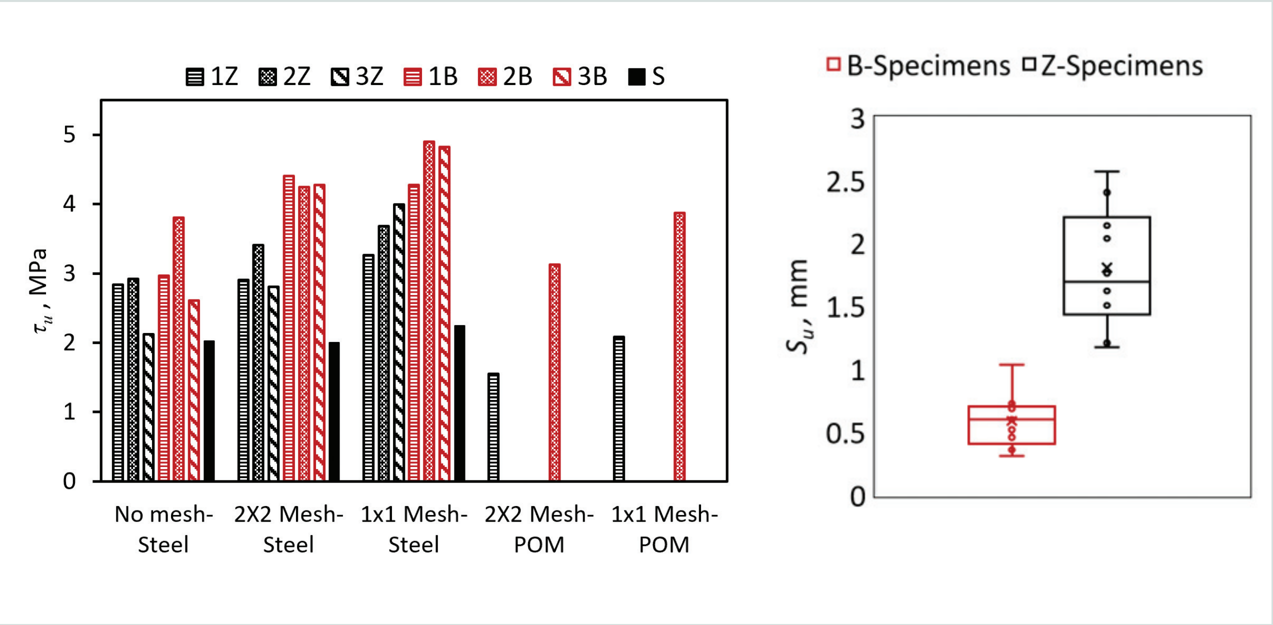

Figure 16. Comparison of peak bond strength τ_u for B and Z specimens compared with S specimens and slip at peak bond strength S_u for B and Z specimens. Note: POM = polyoxymethylene. 1 mm = 0.0394 in.; 1 MPa = 0.145 ksi.

from 0.21 to 1.01 mm (0.01 to 0.04 in.) for steel fibers and up to 1.05 mm (0.04 in.) for POM. This is attributed to the brittle sudden bond failure of the B specimens.

General model

Equations (2) through (4) present a model for peak bond strength specifically for bubbled textures, building on the equation recommended by Liu et al.[16] In this section, the combined data of both surface deformations are used to develop a general model for both bubble-textured and corrugated interfaces of UHPC tubes with steel fibers, as given by Eq. (5):

$$\frac{\tau_u}{\sqrt{f'_{c,n}}} = 1.02 + 20.4\rho_{c,uh} - 0.013(t-a) - 0.15\left(\frac{a}{s}\right) \qquad (5)$$

where

t = total wall thickness

a = protrusion of the deformation = a_b for bubbles and a_z for corrugation

s = spacing of deformation = x_b for bubbles and d_z for corrugations

Figure 17 shows the performance of this equation against the experimental results, where most of the data fit within ±20% margins.

Conclusion

This study investigated the bond performance between prefabricated UHPC tubes and NSC cores for composite columns.

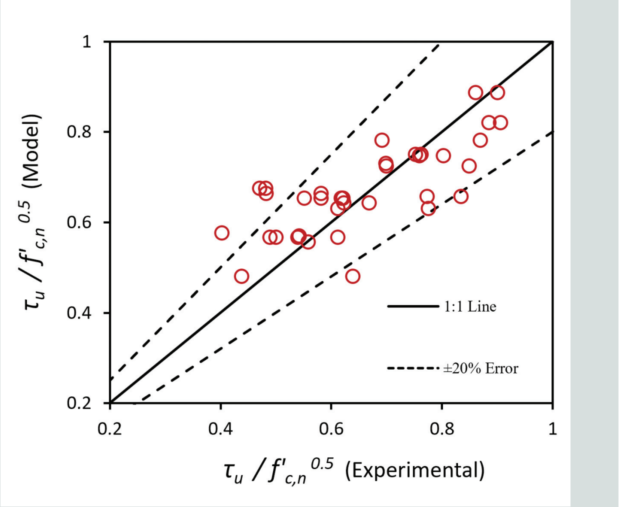

Figure 17. Predicted compared with experimental peak bond strength τ_u for ultra-high-performance concrete tubes with steel fibers and bubbled or corrugated textures. Note: $f'_{c,n}$ = compressive strength of normal-strength concrete.

Two interface types were examined: bubble textured (B specimens) and corrugated (Z specimens). Both were compared with control specimens with smooth interfaces (S specimens). The study also varied UHPC hoop reinforcement ratio $\rho_{c,uh}$, fiber type, and NSC strength $f'_{c,n}$. The bond-slip responses, failure modes, peak bond strength τ_u, and residual bond strength τ_r were evaluated. The study found that average τ_u ranged from 1.6 to 4.9 MPa (0.23 to 0.71 ksi) for deformed interfaces, compared with 2.0 to 2.3 MPa (0.29 to 0.33 ksi) for smooth interfaces. Average τ_r ranged from 0.0 to 2.0 MPa.

Empirical models were developed for τ_u. These experiments resulted in the following findings:

- Bubbles produced nearly cylindrical recesses in UHPC tubes and increased τ_u by 29% to 120%, while vertical corrugations increased τ_u by 0% to 78%, relative to the smooth surface, depending on bubbles or corrugations size, fiber type, $\rho_{c,uh}$ of the tube, and $f'_{c,n}$ of the NSC. However, these deformations reduced τ_r substantially.

- Hoop reinforcement ratio $\rho_{c,uh}$ in a UHPC tube affected τ_u more significantly with deformed interfaces (bubbles or corrugations) than with smooth interfaces. This can be attributed to the induced internal pressure from mechanical interlocking, analogous to the bond of deformed reinforcing bar embedded in concrete.

- Medium-sized bubble recesses of 25 mm diameter and 8 mm rise (25 × 8 mm [1.0 × 0.31 in.]) in UHPC tubes with steel fibers produced higher τ_u than the smaller (10 × 4 mm [0.39 × 0.16 in.]) and larger (30 × 13 mm [1.18 × 0.51 in.]) recesses; however, the smallest (10 × 4 mm) produced the highest τ_r.

- Medium-sized wavy corrugations with 10 mm pitch and 5 mm amplitude (10 × 5 mm [0.39 × 0.20 in.]) in UHPC tubes with steel fibers mostly produced higher τ_u than the smaller (6 × 7 mm [0.24 × 0.28 in.]) and the larger (15 × 3 mm [0.59 × 0.12 in.]) corrugations. No specific trend was observed for their effect on τ_r. While bubble rise increased with diameter, corrugation amplitude reduced with pitch.

- Compared with the control specimens, the (25 × 8 mm) bubbles increased τ_u by 88%, 112%, and 119% for $\rho_{c,uh}$ of 0%, 0.46%, and 0.93%, respectively, while the (10 × 5 mm) corrugations increased τ_u by 44%, 70%, and 64%, respectively, for similar $\rho_{c,uh}$ ratios.

- POM fibers reduced τ_u. For the same $\rho_{c,uh}$, τ_u in tubes with POM fibers decreased by 21% to 26% in bubbled interfaces and by 36% to 47% in corrugated interfaces, respectively, compared with their counterparts with steel fibers.

- Increasing $f'_{c,n}$ of the NSC core by 55% increased τ_u by 18% to 22%, depending on the $\rho_{c,uh}$ of the UHPC tube.

- Failure of NSC-filled bubbled protrusions of all sizes and small and medium corrugations (6 and 10 mm [0.24 and 0.39 in.] pitches, respectively) was by direct shear, whereas large corrugations with 15 mm pitch slipped over without shearing. These were accompanied by longitudinal cracking of the UHPC tube that ranged from hairline cracks in small deformations to full splitting and even UHPC reinforcement rupture with large deformations.

Acknowledgments

The authors wish to acknowledge the financial contributions of the Natural Sciences and Engineering Research Council of Canada (NSERC).

References

1. Hung, C.-C., and C.-H. Yen. 2021. "Compressive Behavior and Strength Model of Reinforced UHPC Short Columns." *Journal of Building Engineering* 35. https://doi.org/10.1016/j.jobe.2020.102103.

2. Farouk, A. I. B., W. Rong, and J. Zhu. 2023. "Compressive Behavior of Ultra-High-Performance–Normal Strength Concrete (UHPC-NSC) Column with the Longitudinal Grooved Contact Surface." *Journal of Building Engineering*, no. 68. https://doi.org/10.1016/j.jobe.2023.106074.

3. Al-Osta, M. A., A. M. Sharif, A. C. M. Suhoothi, and S. K. Najamuddin. 2021. "Strengthening of Axially and Eccentrically Compression Loaded RC Columns with UHPC Jacketing System: Experimental Investigation and Finite Element Modeling." *Engineering Structures*, no. 245. https://doi.org/10.1016/j.engstruct.2021.112850.

4. Farzad, M., A. Sadeghnejad, S. Rastkar, A. Moshkforoush, and A. Azizinamini. 2020. "A Theoretical Analysis of Mechanical and Durability Enhancement of Circular Reinforced Concrete Columns Repaired with UHPC." *Engineering Structures*, no. 209. https://doi.org/10.1016/j.engstruct.2019.109928.

5. Huang, Y., M.-G. Lee, Y.-C. Kan, W.-C. Wang, Y.-C. Wang, and W.-B. Pan. 2022. "Reinforced Concrete Beams Retrofitted with UHPC or CFRP." *Case Studies in Construction Materials*, no. 17. https://doi.org/10.1016/j.cscm.2022.e01507.

6. Liu, T., and J.-P. Charron. 2023. "Experimental Study on the Shear Behavior of UHPC-Strengthened Concrete T-Beams." *Journal of Bridge Engineering* 28 (9). https://doi.org/10.1061/JBENF2.BEENG-6122.

7. Abbas, H. M., M. M. A. Kadhim, and A. Jawdhari. 2025. "Prefabricated GFRP-Reinforced UHPC Overlays for Strengthening RC Beams in Flexure." *Structural Concrete*. https://doi.org/10.1002/suco.70399.

8. Haber, Z. B., J. F. Munoz, I. De La Varga, and B. A. Graybeal. 2018. "Bond Characterization of UHPC Overlays for Concrete Bridge Decks: Laboratory and Field Testing." *Construction and Building Materials*, no. 190, 1056–1068. https://doi.org/10.1016/j.conbuildmat.2018.09.167.

9. Hussein, H. H., K. K. Walsh, S. M. Sargand, and E. P. Steinberg. 2016. "Interfacial Properties of Ultrahigh-Performance Concrete and High-Strength Concrete Bridge Connections." *Journal of Materials in Civil Engineering* 28 (5). https://doi.org/10.1061/(ASCE)MT.1943-5533.0001456.

10. Abbas, S., A. M. Soliman, and M. L. Nehdi. 2015. "Exploring Mechanical and Durability Properties of Ultra-High Performance Concrete Incorporating Various Steel Fiber Lengths and Dosages." *Construction and Building Materials*, no. 75, 429–441. https://doi.org/10.1016/j.conbuildmat.2014.11.017.

11. Yuan, W., X. Wang, Z. Dong, P. Zhou, and Q. Wang. 2022. "Cyclic Loading Test for RC Bridge Piers Strengthened with UHPC Jackets in the Corrosive Environment." *Soil Dynamics and Earthquake Engineering*, no. 158. https://doi.org/10.1016/j.soildyn.2022.107290.

12. Semendary, A. A., W. K. Hamid, E. P. Steinberg, and I. Khoury. 2020. "Shear Friction Performance between High Strength Concrete (HSC) and Ultra High Performance Concrete (UHPC) for Bridge Connection Applications." *Engineering Structures*, no. 205. https://doi.org/10.1016/j.engstruct.2019.110122.

13. Abellán-García, J., J. S. Carvajal-Muñoz, and C. Ramírez-Munévar. 2024. "Application of Ultra-High-Performance Concrete as Bridge Pavement Overlays: Literature Review and Case Studies." *Construction and Building Materials*, no. 410. https://doi.org/10.1016/j.conbuildmat.2023.134221.

14. Fakeh, M., and A. Fam. 2026. "Behavior of RC Columns Encased by Precast UHPC Tubes with Corrugated Surface under Bending and Axial Loads." *Journal of Structural Engineering*. Under review.

15. Jang, H.-O., H.-S. Lee, K. Cho, and J. Kim. 2017. "Experimental Study on Shear Performance of Plain Construction Joints Integrated with Ultra-High Performance Concrete (UHPC)." *Construction and Building Materials*, no. 152, 16–23. https://doi.org/10.1016/j.conbuildmat.2017.06.156.

16. Liu, J., Z. Chen, D. Guan, Z. Lin, and Z. Guo. 2020. "Experimental Study on Interfacial Shear Behaviour between Ultra-High Performance Concrete and Normal Strength Concrete in Precast Composite Members." *Construction and Building Materials*, no. 261. https://doi.org/10.1016/j.conbuildmat.2020.120008.

17. Fakeh, M., and A. Fam. 2026b. "Bond between Circular UHPFRC Jackets for Columns and Concrete Core at Different Temperatures." *Construction and Building Materials*, no. 522. https://doi.org/10.1016/j.conbuildmat.2026.145968.

18. Yu, R., K. Liu, T. Yin, L. Tang, M. Ding, and Z. Shui. 2022. "Comparative Study on the Effect of Steel and Polyoxymethylene Fibers on the Characteristics of Ultra-High Performance Concrete (UHPC)." *Cement and Concrete Composites*, no. 127. https://doi.org/10.1016/j.cemconcomp.2022.104418.

19. ASTM (American Society for Testing Materials). 2021. *Test Method for Compressive Strength of Cylindrical Concrete Specimens*. ASTM C39–21. West Conshohocken, PA: ASTM International. http://www.astm.org/cgi-bin/resolver.cgi?C39C39M-21.

20. Fakeh, M., and A. Fam. 2026c. "Split-Disk Testing of Precast Ultra-High Performance Fiber-Reinforced Concrete Tubes." *Structural Concrete*. https://doi.org/10.1002/suco.70554.

21. Graybeal, B. A. 2006. *Material Property Characterization of Ultra-High Performance Concrete*. Report FHWA-HRT-06-103. Washington, DC: Federal Highway Administration, U.S. Department of Transportation.

22. Horák, P., Š. Pešková, M. Jogl, R. Sovják, and P. Vítek. 2022. "Experimental Investigation of Cohesion between UHPC and NSC Utilising Interface Protrusions." *Materials* 15 (19). https://doi.org/10.3390/ma15196537.

Notation

a = protrusion of deformation

a_b = bubble rise

a_z = corrugation amplitude

$A_{b,t}$ = bubble area at shear level

A_s = interface surface area

d_b = bubble diameter

d_z = corrugation pitch

D_i = inside diameter of ultra-high-performance concrete tube

D_o/t_e = outer diameter-to-equivalent thickness ratio

E_s = modulus of elasticity of steel

f'_c = compressive strength

$f'_{c,n}$ = compressive strength of NSC

$f'_{c,u}$ = compressive strength of UHPC

f_u = tensile strength of steel

f_y = yield stress of steel

H_b = bonded region height

H_t = height of UHPC tubes

K_b = confinement factor

P = applied load

s = spacing of deformation

S = slip

S_u = slip at peak bond strength

t = total wall thickness

t_e = equivalent thickness

V_b = volume of bubble or corrugation

x_b = center-to-center bubble distance

$\rho_{c,uh}$ = hoop reinforcement ratio

τ = bond stress

τ_u = peak bond strength

τ_{uo} = reference shear/bond strength

τ_r = residual bond strength

About the authors

Mina Fakeh is a PhD graduate from the Department of Civil Engineering at Queen's University in Kingston, ON, Canada.

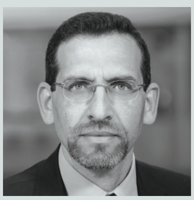

Amir Fam is a Tier I Canada Research Chair Professor in Climate Change Resilient Infrastructure in the Department of Civil Engineering at Queen's University.

Abstract

This study investigated the bond behavior between prefabricated ultra-high-performance concrete (UHPC) tubes and normal-strength concrete (NSC) fill using push-out tests. Bubble-textured and corrugated interfaces were examined and compared with control specimens with a smooth interface. UHPC hoop reinforcement ratio $\rho_{c,uh}$, fiber type, and NSC strength $f'_{c,n}$ were also varied. The study found that peak bond strength τ_u ranged from 1.6 to 4.9 MPa (0.23 to 0.71 ksi) for deformed interfaces, compared with 2.0 to 2.3 MPa (0.29 to 0.33 ksi) for smooth interfaces, while residual bond strength τ_r ranged from 0.0 to 2.0 MPa. Bubbled texture with steel fibers increased τ_u by 29% to 120%, while corrugations increased τ_u by 5% to 78%; however, these deformations reduced τ_r substantially. Medium-sized bubble recesses of 25 mm diameter and 8 mm rise (25 × 8 mm [1.0 × 0.31 in.]) and wavy corrugations of 10 mm pitch and 5 mm amplitude (10 × 5 mm [0.39 × 0.20 in.]) produced the highest τ_u. The 25 × 8 mm bubbles increased τ_u by 88%, 112%, and 119% for UHPC $\rho_{c,uh}$ of 0%, 0.46%, and 0.93%, respectively, while the 10 × 5 mm corrugations increased τ_u by 44%, 70%, and 64%, respectively, for similar $\rho_{c,uh}$ ratios. POM fibers reduced τ_u, compared with steel fibers, by 21% to 26% in bubbled interfaces and by 36% to 47% in corrugated interfaces, respectively. Failure of NSC-bubbled protrusions of all sizes and small and medium corrugations was by direct shear, whereas large corrugations slipped over without shearing. Failure was generally accompanied by longitudinal cracking of the UHPC tube, ranging from hairline cracks in small deformations to full splitting and even UHPC reinforcement rupture in large deformations. Empirical models were developed for τ_u.

Keywords

Bond, bubble, corrugation, deformation, interface, normal-strength concrete, smooth, UHPC, ultra-high-performance concrete.

Review policy

This paper was reviewed in accordance with the Precast/Prestressed Concrete Institute's peer-review process. The Precast/Prestressed Concrete Institute is not responsible for statements made by authors of papers in *PCI Journal*. No payment is offered.

Publishing details

This paper appears in *PCI Journal* (ISSN 0887-9672) V. 71, No. 5, September–October 2026, and can be found at https://doi.org/10.15554/pcij71.5-02. *PCI Journal* is published bimonthly by the Precast/Prestressed Concrete Institute, 8770 W. Bryn Mawr Ave., Suite 1150, Chicago, IL 60631.

Reader comments

Please address any reader comments to journal@pci.org or Precast/Prestressed Concrete Institute, c/o *PCI Journal*, 8770 W. Bryn Mawr Ave., Suite 1150, Chicago, IL 60631.